GROOVE STIFFENING OF SHEETS BY SINGLE POINT INCREMENTAL FORMING: EXPERIMENTAL AND NUMERICAL INVESTIGATION

Valentino A.M. Cristino[a], João P.M. Pragana[b], Ivo M.F. Bragança[c], Carlos M.A. Silva[b], Paulo A.F. Martins[b,]*

[a]Department of Electromechanical Engineering, University of Macao, Avenida da Universidade, Taipa, Macao
[b]IDMEC, Instituto Superior Técnico, Universidade de Lisboa, Portugal
[c]CIMOSM, Instituto Superior de Engenharia de Lisboa, Instituto Politécnico de Lisboa, Portugal

First author. E-mail: vcristino@um.edu.mo
Second author. E-mail: joao.pragana@tecnico.ulisboa.pt
Third author. E-mail: ibraganca@dem.isel.ipl.pt
Fourth author. E-mail: carlos.alves.silva@tecnico.ulisboa.pt
Corresponding author. E-mail: pmartins@tecnico.ulisboa.pt Telephone: +351218419006

ABSTRACT

This paper investigates the applicability of single point incremental forming (SPIF) to produce stiffening grooves in thin metal panels. The work combines experimentation and modelling using finite element analysis and a new analytical model based on in-plane membrane stretching to determine the required forming forces and to estimate the maximum allowable groove depths that can be produced without tearing. The presentation shows that single point incremental forming can easily and effectively produce stiffening grooves that are an alternative to conventional reinforcements made from stringers that are welded, riveted, or rigidly fastened to the panel surfaces. Results obtained from the analytical model are compared against experimental measurements and finite element predictions to prove its effectiveness in replicating the deformation mechanics of groove stiffening by single point incremental forming.

Keywords: Single point incremental forming; stiffening grooves; analytical modelling; finite element method; experimentation

1. INTRODUCTION

Stretching is a metal forming process in which a sheet gripped along its edges, is simultaneously stretched, bent, and thinned by a punch to achieve the desired final geometry (Figure 1a). The process is widely used in aerospace, automotive, shipbuilding and civil construction to fabricate panels with different surfaces and thicknesses [1].

The production and utilization of panels made from thin sheets (hereafter referred to as 'thin panels') often require reinforcement by means of stringers (Figure 1b) that can be subsequently welded, riveted, or rigidly fastened to their surfaces.

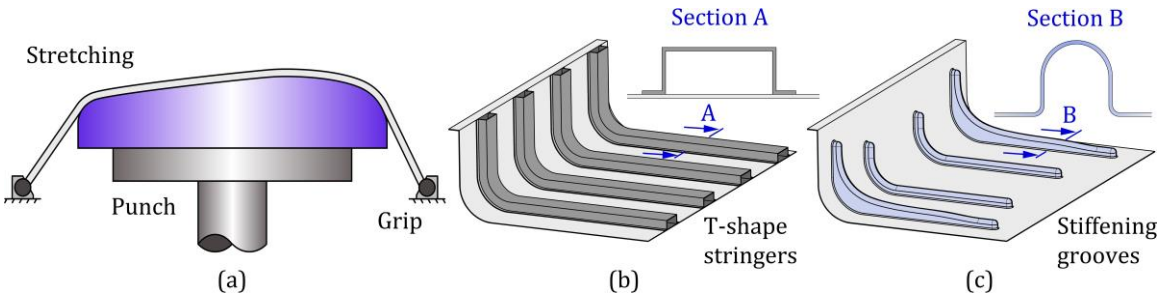

Figure 1 (a) Stretching of thin panels and strengthening by means of (b) longitudinal 'T-shape' stringers and (c) longitudinal stiffening grooves.

The alternative of reinforcing the thin panels with stringers before stretching is usually not an option due to the possibility of cracking and buckling caused by the tensile or compressive stresses that are induced in the stringers and panels during plastic deformation. To make this alternative viable for industrial implementation, Köhler et al. [2] recently proposed a solution based on a cam-actuated mechanism that can assemble the stringers on the panels before stretching. The solution successfully prevents the occurrence of buckling by providing lateral support of the stringers during stretching, but gives rise to new failure modes, and significant amounts of spring back after forming. Moreover, it increases the complexity and cost of the tools and manufacturing routes, when compared to existing solutions based on conventional stretching and reinforcement by means of stringers that are welded, riveted, or fastened.

Resort to manufacturing solutions where the panels and reinforcements are milled from a single billet, allows producing thin monolithic (homogeneous) panels with integrated stringers having excellent strength-to-weight ratios and substantial cost savings in assembly, labor, and tooling. In fact, thin monolithic panels eliminate the use of rivets or screws as well as the metallurgical changes in the heat-affected zones and the thermal-induced distortions resulting from welding that create difficulties in obtaining the desired final geometry and performance of the panels.

The main drawbacks associated to the fabrication of thin monolithic panels are the final surface roughness, the overall machining time, and the big waste of material, which can account for more than 95% of the initial billet [3, 4]. Still, this type of panels is commonly used in aerospace applications.

Other manufacturing solutions based on conventional forming of grooves with punch and die sets [5, 6] are limited by the time and cost to fabricate the tools and because the tools are dependent on the geometry of the panels. Despite electromagnetic forming allows one element of the set of tools (usually the punch) to be replaced by a coil, this process variant is limited to highly conductive materials, to small size panels and cannot avoid the groove geometry dependence of the dies [7].

This paper explores the potential of using single-point incremental forming (SPIF) to emboss stiffening grooves with moderate-to-high depths and thickness changes in thin panels (Figure 1c), as it was originally proposed by Slota et al. [8]. Stiffening grooves are a special type of reinforcements that are produced by local pressing of the sheet panels during forming in a single clamping SPIF operation. The possibility of performing the forming and stiffening stages simultaneously combined with the dieless characteristics of SPIF, leads to greater flexibility and economic benefits than those currently offered by conventional reinforcement by stringers.

The work to be presented in this paper combines experimentation with commercial AISI 316L stainless steel sheets and modelling using a commercial finite element software and

an analytical framework developed by the authors [9] to predict the forming force and the maximum admissible groove depth. Results prove not only the feasibility of SPIF to fabricate stiffening grooves in thin metal panels but also the good quality of the plastic deformation estimates obtained by means of the new proposed analytical model.

2. MATERIALS AND METHODS

2.1 Mechanical characterization

The work was carried out in AISI 316L stainless steel sheets with 1 mm thickness. The mechanical properties and flow curve of the material were determined by means of tensile tests on an INSTRON 5900 universal testing machine, according to the ASTM standard E8/E8 M-16 [10]. The specimens were cut out from the supplied sheets at 0°(P-parallel), 45°(I-inclined) and 90°(T-transversal) inclination with respect to the rolling directions and Figure 2 and Table 1 summarize the results obtained from these tests.

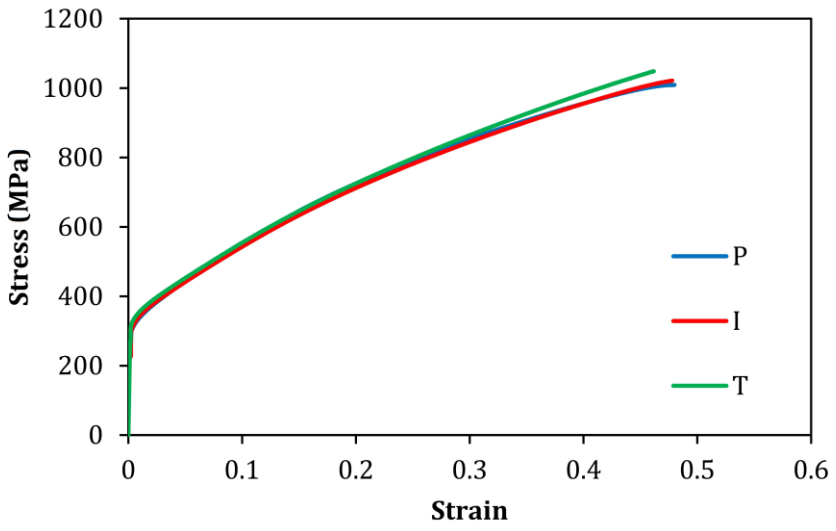

Figure 2 True stress–strain curves of AISI 316L stainless steel sheets for the parallel (P), inclined (I) and transverse (T) directions with respect to the rolling directions.

Table 1. Mechanical properties of the AISI 316L stainless-steel sheets.

Material	Direction	Yield stress (MPa)	Elongation at break (%)	Anisotropy coefficient
AISI 316L	P	320.7 ± 4.4	64.9 ± 3.3	0.94
	I	313.5 ± 3.1	63.6 ± 3.5	0.97
	T	310.5 ± 3.8	61.2 ± 4.1	0.98
Average values		312.25	63.33	0.97

2.2 Experimentation

Groove stiffening by SPIF was carried out in sheet specimens with a geometry of 130 mm x 50 mm x 1 mm. The experimental setup to fabricate the stiffening grooves is shown in Figure 3. and consists of: (a) a forming tool with a semi-hemispherical tip of 6 mm radius, made from a cold working alloy tool steel with chromium, vanadium, and tungsten (120WV4—DIN), hardened and tempered to 60 HRC; (b) a backing plate and (c) a screw-loaded pressure pad located at the outer perimeter of the sheet.

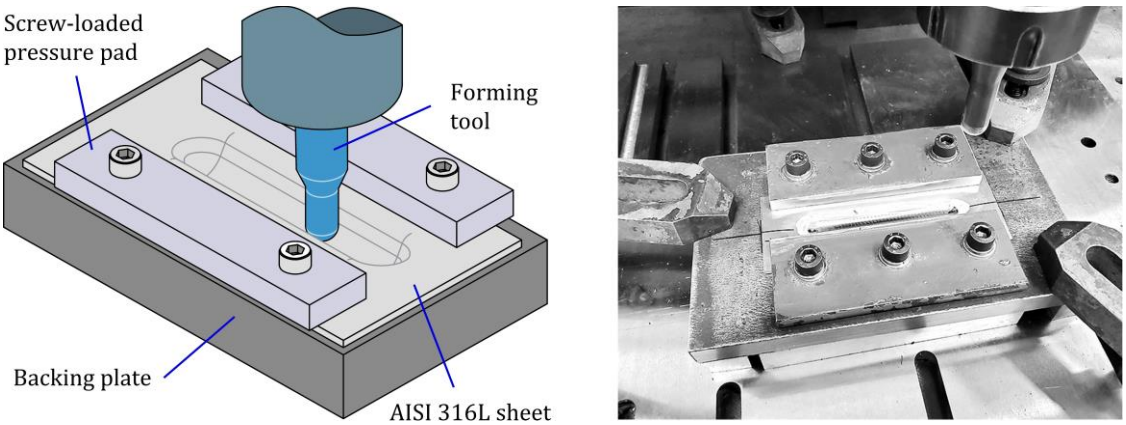

Figure 3 Schematic representation and photograph of the experimental setup to fabricate the stiffening grooves by SPIF under laboratory conditions.

SPIF was carried out with a reciprocating straight tool path along the longitudinal direction and a vertical step size of 1 mm per tool path. The tool feed rate and rotation were set equal to 200 mm/min and 100 rpm, respectively.

A ceramic grease Weicon ASW 040P was applied on the tool-sheet interface for lubrication.

All the sheet specimens were electrochemically etched with a grid of overlapping circles having an initial diameter of 2 mm for allowing measuring the major and minor axis of the ellipses and quantifying the in-plane strains ($\varepsilon_\phi, \varepsilon_z$) resulting from plastic deformation of the circles (a procedure known as 'circle grid analysis' [11]). The measurements were performed for various groove depth H configurations with a computer-aided system consisting of a 3Com USB camera and the GPA 3.0 software.

2.3 Finite element analysis

Finite element simulation of groove stiffening by SPIF was carried out with the commercial software LS-DYNA. The sheet specimens were modelled as elastic-plastic deformable objects and discretized by means of adaptive meshes consisting of 6500 shell elements with approximately 1 mm x 1 mm initial size and five integration points through thickness (Figure 4a). The semi-hemispherical tip forming tool and the backing plate were modelled as rigid objects and the tool moving path was set identical to that of the actual SPIF process. The AISI 316L stainless-steel sheet specimens were assumed as isotropic ($r \cong 1$) and material strain hardening was characterized by means of an average Ludwik-Hollomon power law resulting from the tensile tests performed in different directions (Table 1).

The simulations were performed with a load factoring (or time-scaling) procedure to reduce the overall CPU time, which was approximately equal to 5 hours in a computer equipped with an Intel i7-6700 (3.4 GHz) processor.

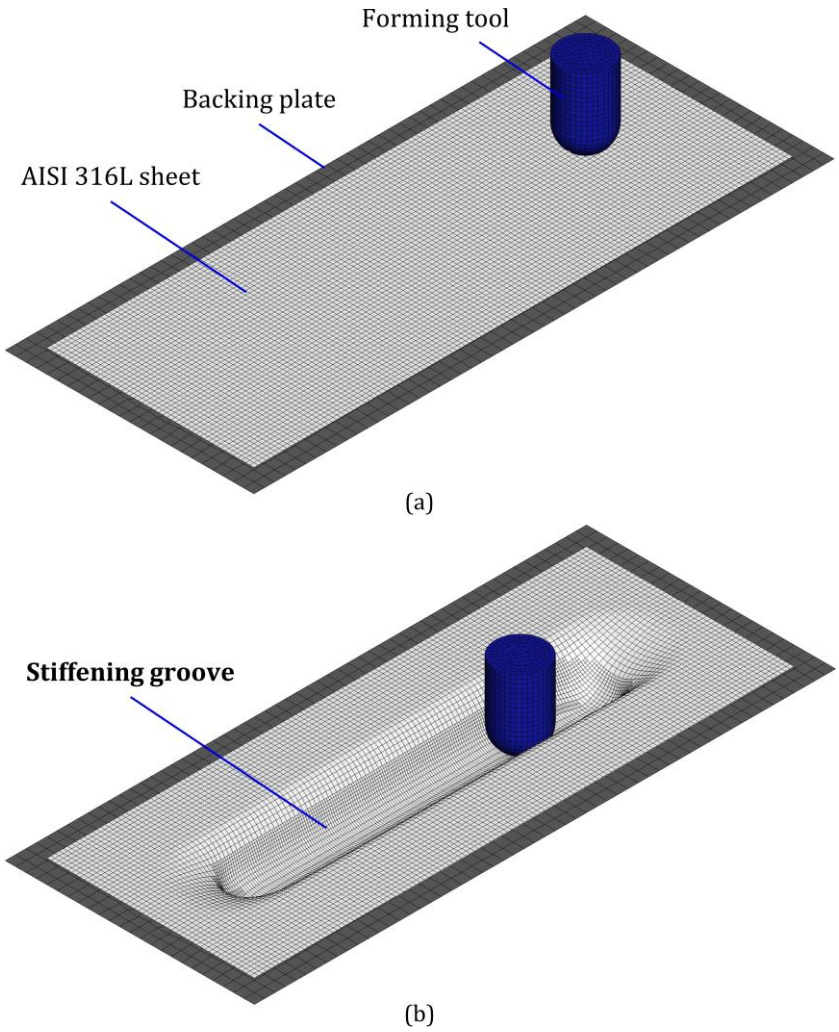

Figure 4 (a) Initial and (b) final computed meshes obtained from finite element analysis.

2.4 Analytical model

Experimental observations (refer to Section 3) of groove stiffening by SPIF showed that material deforms under plane strain loading conditions ($\beta = d\varepsilon_z/d\varepsilon_\phi = 0$), except at the entry and exit of the tool during which material flows under biaxial stretching loading conditions ($\beta = d\varepsilon_z/d\varepsilon_\phi = 1$). The analytical model to be presented in this section is limited to steady-state, plane-strain material flow conditions.

A typical cross-section of a stiffening groove is shown in Figure 5 and consists of a shell, assumed as a membrane, so that bending moments are neglected and forces are essentially transmitted through the sheet surfaces subjected to in-plane stretching. Three-main regions can be identified in Figure 5a: (i) the wrap angle θ around the semi-hemispherical tool,

(ii) the straight unsupported surface with a length L_s making an angle α_s with the tool center and (iii) the curvature radius R_b at the transition between the undeformed and the plastically deformed material.

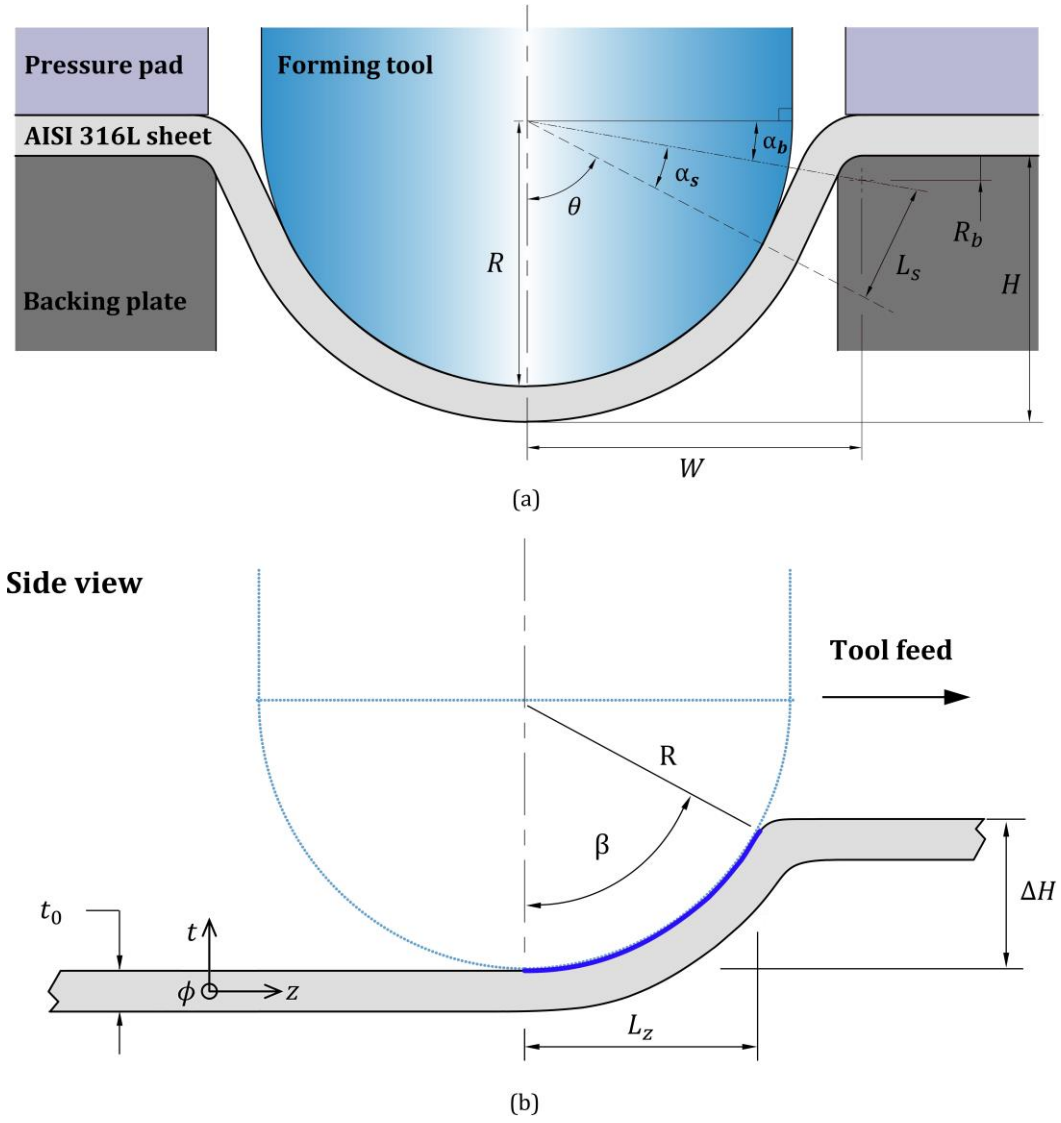

Figure 5 (a) Schematic representation of the stiffening groove with main notation; (b) the corresponding area of the local contact between the tool and the sheet placed immediately ahead.

The wrap angle θ around the semi-hemispherical tool is given by,

$$\theta = \frac{\pi}{2} - \alpha_s - \alpha_b \tag{1}$$

where the angles α_s and α_b of the straight unsupported surface and of the transition between the undeformed and the plastically deformed material are related with the radius of the semi-hemispherical tool R,and the depth H and width W of the groove, as follows,

$$\alpha_b = arctan\left(\frac{R - H + R_b}{W}\right) \tag{2}$$

$$\alpha_s = arccos\left(\frac{R_b + R}{\sqrt{\{W^2 + (R - H + R_b)^2\}}}\right) \tag{3}$$

The analytical model considers the meridional (ϕ), thickness (t) and longitudinal (z) directions as principal directions and deformation to take place under plane stress $\sigma_t = 0$ loading conditions along the thickness direction, as it is commonly assumed in sheet metal forming.

Average meridional strain

The material of the sheet specimens is assumed as isotropic (Table 1) and rigid plastic (i.e., no elastic effects are included) with strain hardening following the Ludwik-Hollomon relationship $\bar{\sigma} = k\bar{\varepsilon}^n$. Under these conditions, the effective strain $\bar{\varepsilon}$ along the perimeter of the stiffening groove and the corresponding meridional stress σ_ϕ can be directly obtained from the meridional strain ε_ϕ as follows,

$$\begin{aligned} \bar{\varepsilon} &= \frac{2}{\sqrt{3}}\varepsilon_\phi \\ \sigma_\phi &= \frac{2}{\sqrt{3}}\,\bar{\sigma} \end{aligned} \tag{4}$$

The meridional strain ε_ϕ in (4) can be determined from experimental circle grid analysis, finite element simulation and from the analytical model under consideration. In case of the latter, it requires determining the evolution of the half-perimeter of the groove L_ϕ for an

arbitrary depth H during stretching following a procedure like that earlier developed by Martins and Marques [12] for conventional stretching with a cylindrical punch.

$$L_\phi = (R + R_b)\theta + L_s \tag{5}$$

where the length L_s of straight unsupported groove length is given by,

$$L_s = \sqrt{\{W - (R + R_b)sin\theta\}^2 + \{H - (R + R_b)(1 - cos\theta)\}^2} \tag{6}$$

In the above equation, W is the original (undeformed) sheet length from where the groove is plastically formed.

Under these circumstances, the average value of the meridional strain ε_ϕ^{avg} in the groove is obtained from,

$$\varepsilon_\phi^{avg} = ln\left(\frac{L_\phi}{W}\right) \tag{7}$$

Forming force

The forming force F necessary for the fabrication of stiffening grooves by SPIF is determined from,

$$F = 2\sigma_\phi^{avg} t_0 L_z sin\theta exp\left(-\varepsilon_\phi^{avg}\right) \tag{8}$$

where t_0 is the undeformed sheet thickness, L_z is the contact length in the z-direction (Figure 5b) and σ_ϕ^{avg} is the average meridional stress, which in turn can be determined from the increments of average meridional strain $d\varepsilon_\phi^{avg}$ within successive configurations (under plane stress conditions along the thickness direction $\sigma_t = 0$),

$$\sigma_{\phi}^{avg} = \frac{4}{3}\frac{\bar{\sigma}}{d\bar{\varepsilon}} d\varepsilon_{\phi}^{avg} \tag{9}$$

Maximum allowable depth

The maximum allowable groove depth H is determined by combining the average meridional strain ε_{ϕ}^{avg} (7) with the constitutive equations relating the increments of strain with the applied stresses under combined plane strain ($\varepsilon_z = 0$) and plane stress ($\sigma_t = 0$) deformation conditions,

$$\begin{aligned} d\varepsilon_{\phi} &= \frac{1}{2}\frac{d\bar{\varepsilon}}{\bar{\sigma}}\left[2\sigma_{\phi} - \sigma_z\right] \\ d\varepsilon_z &= \frac{1}{2}\frac{d\bar{\varepsilon}}{\bar{\sigma}}\left[2\sigma_z - \sigma_{\phi}\right] = 0 \\ d\varepsilon_t &= \frac{1}{2}\frac{d\bar{\varepsilon}}{\bar{\sigma}}\left[-\sigma_z - \sigma_{\phi}\right] \end{aligned} \tag{10}$$

This procedure allows writing the average distributions of thickness strain ε_t^{avg} and longitudinal stress σ_z^{avg} for an arbitrary groove depth H, as follows,

$$\varepsilon_t^{avg} = -\varepsilon_{\phi}^{avg} \tag{11}$$

$$\sigma_z^{avg} = \frac{1}{2}\sigma_{\phi}^{avg} \tag{12}$$

and determining the average thickness t^{avg} of the groove by means of,

$$t^{avg} = t_0 exp\left(-\varepsilon_t^{avg}\right) \tag{13}$$

To determine the maximum allowable groove depth H_{max} it is first assumed that material strain hardening tends to balance the reduction in thickness so that the force per unit of length $T_\phi = \sigma_\phi t$ in the meridional direction can be assumed as constant. This assumption earlier employed by Cristino et al. [9] facilitates analytical modelling and is commonly employed in membrane analysis of sheet metal forming processes [13].

Under these assumptions, the force per unit of length T_ϕ is expected to have a constant value C for each groove depth H, which can be determined by combining equations (9) and (13),

$$T_\phi = \sigma_\phi^{avg} t^{avg} = C \tag{14}$$

The fracture forming limit (FFL) of the AISI 316L sheets was previously determined by the authors [9] and allow identifying the critical meridional strain ε_ϕ^{crit} at the onset of cracking, from which the minimum sheet thickness t_{min} can be obtained by employing equation (13) for critical values instead of average values,

$$t_{min} = t_0 exp\left(-\varepsilon_t^{crit}\right) \qquad \varepsilon_t^{crit} = -\varepsilon_\phi^{crit} \tag{15}$$

Once the minimum sheet thickness t_{min} of the stiffening groove is obtained and the critical meridional stress σ_ϕ^{crit} is obtained by employing equation (9) for critical values, it is possible to estimate the critical force per unit of length T_ϕ^{crit}, as follows,

$$T_\phi^{crit} = \sigma_\phi^{crit} t_{min} = C^{crit} \tag{16}$$

This last result can then be used to predict the maximum allowable groove depth H_{max}, which corresponds to the instant of time when the force per unit of length T_ϕ (14) is equal to the critical value T_ϕ^{crit} (16) at the onset of failure by fracture.

3. RESULTS AND DISCUSSION

3.1. Shape, thickness, and strain path evolutions

Figure 6a presents the experimental, finite element and analytical evolutions of the cross-sectional geometry of the stiffening groove for two different instants of time corresponding to values of depth H equal to 5 mm and 11 mm, respectively. Due to symmetry, only half of the cross-section is shown,

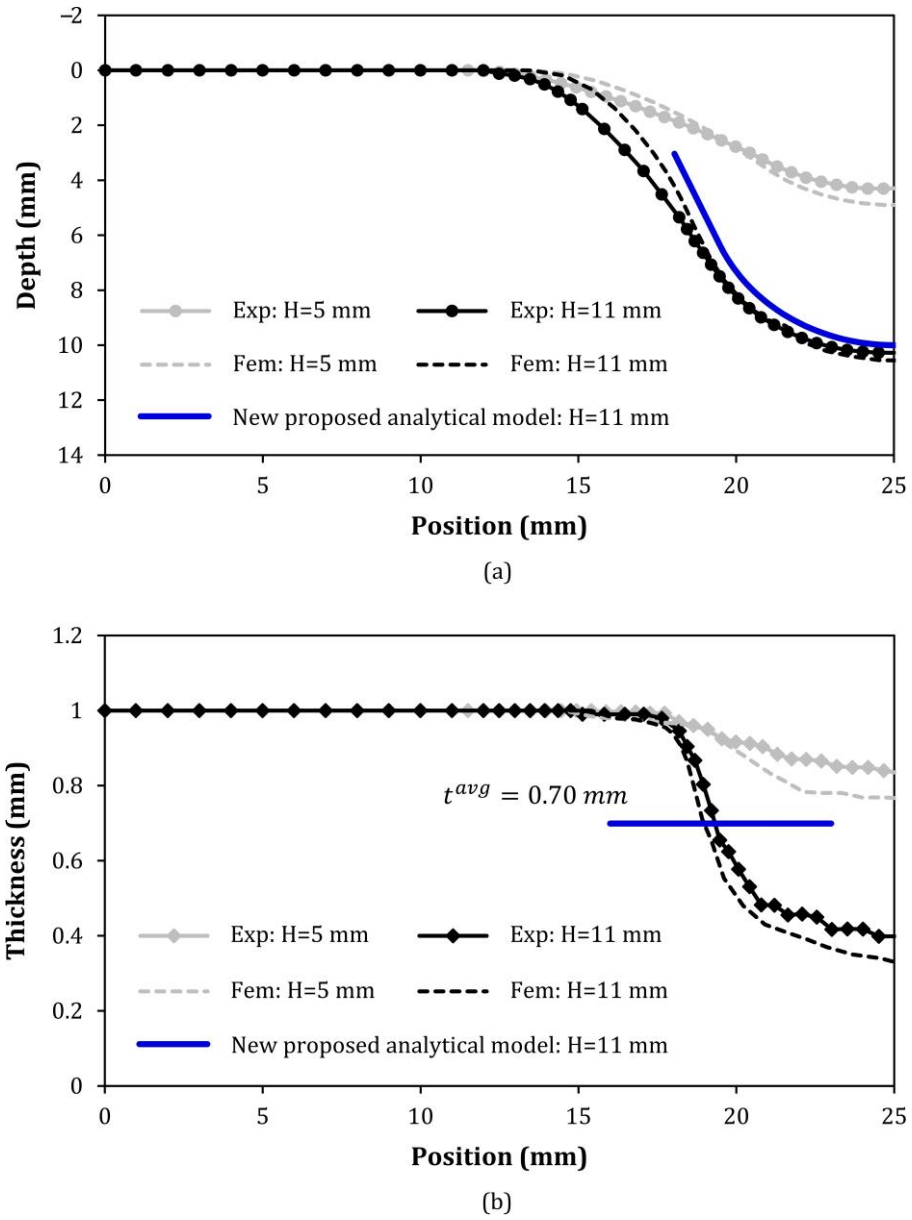

Figure 6 Experimental, numerical, and analytical evolutions of the (a) cross-sectional geometry and (b) thickness of the stiffening groove for two different instants of time corresponding to a groove depth H of the semi-hemispherical tip tool equal to 5 mm and 11 mm

The overall agreement is good and the main differences between the analytical and the experimental and finite element results that are observed in Figure 6a are attributed to the elastic recovery of the stiffening grooves after unloading and halving the sheet specimens lengthwise to reveal their cross-sections and measuring the geometrical profile and thickness. In fact, the elimination of the circumferential constraint due to halving of the sheet specimens is not considered in the finite element simulation.

Figure 6b presents the same type of comparison for the thickness of the stiffening grooves. In this case, the main differences are observed between the analytical and the experimental and finite element results because the former can only provide average thickness t^{avg} (13) values for each groove depth H. However, as will be shown in what follows, this will not compromise the performance of the analytical model for predicting the required forming force and the maximum allowable groove depth.

Figure 7 shows the experimentally measured and the finite element predicted evolutions of the in-plane meridional ε_ϕ and longitudinal ε_z strains along the perimeter of the groove for the instant of time immediately after tearing of the sheet specimens by crack opening and propagation along the longitudinal direction (i.e., tool feed direction). As seen, the in-plane strains fall close to the vertical axis, in close agreement with the earlier assumption that material is subjected to plane strain deformation up to the onset of fracture. Moreover, because no signs of necking are observed in the grooves, as can also be concluded from the observation of the evolution of thickness in Figure 6b, it may be stated that groove stiffening by single point incremental forming fails by critical thickness reduction and crack opening by tension (mode I of fracture mechanics) without previous necking [11].

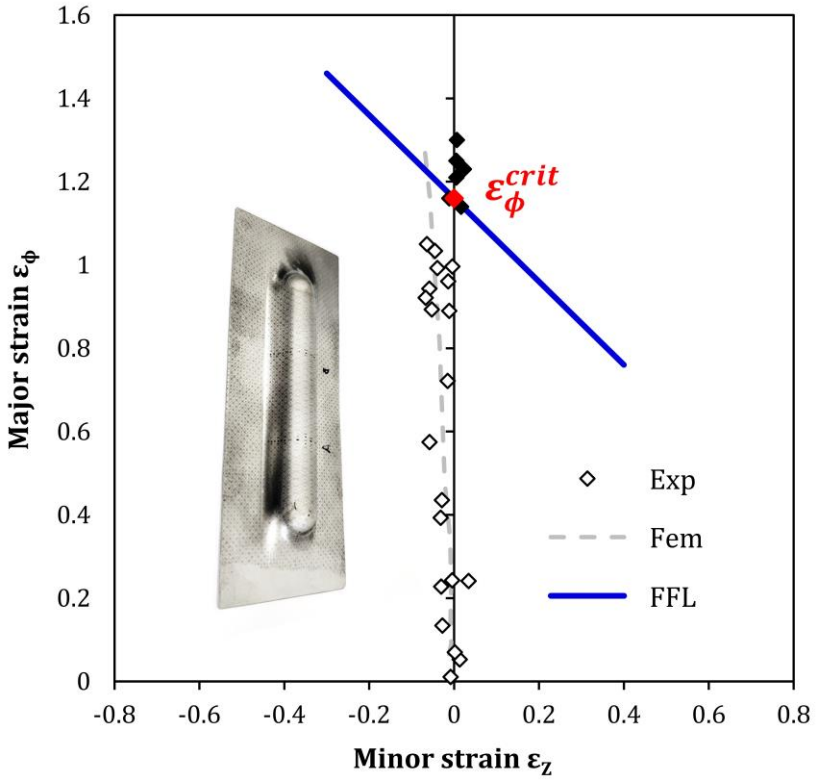

Figure 7 Principal strain space showing the experimental and finite element computed in-plane strains along the perimeter of the stiffening groove for an instant of time corresponding to a depth $H = 14$ mm immediately after cracking.

After validating the shape and thickness obtained from analytical and finite element modelling against experimental values, attention will now be focused on determining the maximum allowable depts of the stiffening grooves and the required forming forces because this information is of paramount importance to the design and fabrication of thin reinforced panels.

3.2. Maximum depth

Combining equations (14) and (4) with the Ludwik-Hollomon strain-hardening relationship $\bar{\sigma} = k\bar{\varepsilon}^n$ for average meridional strain ε_ϕ^{avg} values, it is possible to determine the analytical evolution of the force per unit of length T_ϕ with the stiffening groove depth H as follows,

$$T_\phi = \frac{2}{\sqrt{3}}\,\bar{\sigma}^{avg} t^{avg} = C(H) \qquad \text{with } \bar{\sigma}^{avg} = k\left(\frac{2}{\sqrt{3}}\varepsilon_\phi^{avg}\right)^n \tag{17}$$

The relation given by equation (17) is plotted in Figure 8 and the maximum allowable depth H_{max} is obtained by searching the point in the $T_\phi = C(H)$ evolution that matches the critical value C^{crit} (16) obtained from the onset of failure by fracture based on the critical meridional strain ε_ϕ^{crit} determined from the FFL (Figure 7). The procedure is illustrated in Figure 8 through the intersection between the $T_\phi = C(H)$ evolution and the red dashed horizontal line corresponding to the critical values of force per unit of length T_ϕ^{crit}.

As seen the maximum allowable depth H_{max} obtained from the new proposed analytical model is similar to that predicted by finite elements and slightly above the experimentally measured $H_{max} = 14$ mm.

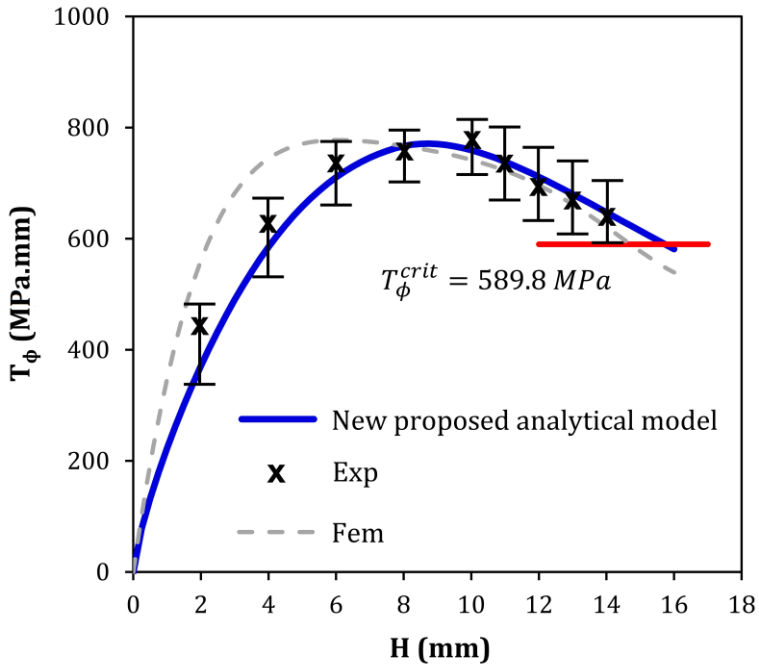

Figure 8 Evolution of the force per unit of length with the groove depth.

3.3. Tool forces

The experimental, analytical, and numerical evolutions of the tool force with the groove depth are shown in Figure 9. As seen, while the predictions obtained by means of finite elements tend to overestimate the experimental values, those obtained from the analytical model tend to underestimate them. Still, both numerical and analytical models are able to

replicate the overall trend of the force vs. depth evolution with differences in the analytical model being attributed to its simplifying assumptions, namely to the utilization of average instead of local values of the main variables and to a certain degree of uncertainty in defining the contact length L_z in the z-direction (Figure 5), because it may include a part of the tool surface located behind the vertical symmetry axis.

Finally, the results provided by the new proposed analytical model were compared against those obtained from a recently proposed analytical model developed by Chang et al. [14]. This other analytical model makes use of the instantaneous wall angle and thickness values for each value of groove depth, which need to be obtained beforehand from the experimental cross-section profiles (or, alternatively, from the corresponding finite element predictions) at different instants of time. However, despite the greater completeness and complexity of this model, the predicted evolution of the forming force with depth is nearly identical to that given by the new proposed analytical model.

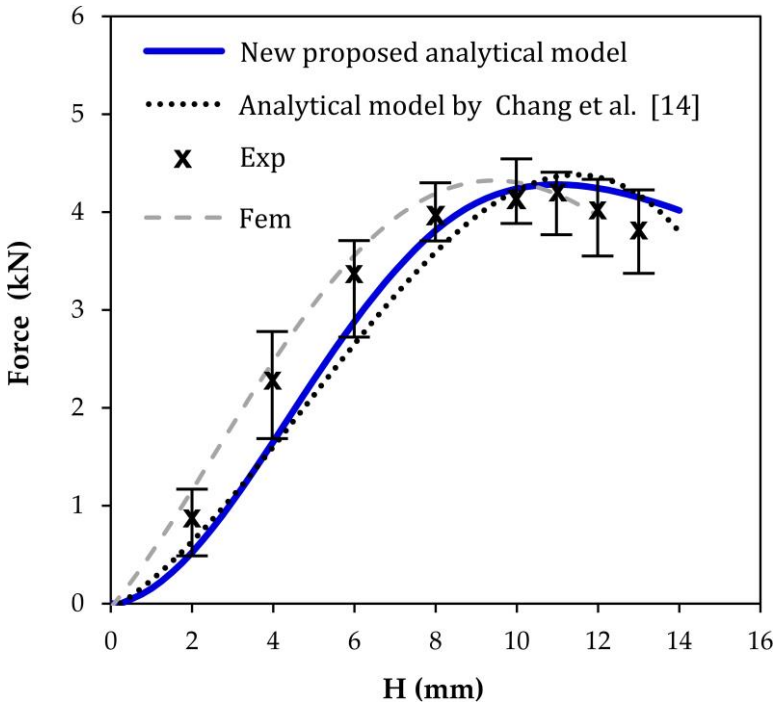

Figure 9 Experimental, numerical, and analytical evolutions of the tool force with the groove depth.

4. CONCLUSIONS

Groove stiffening by single point incremental forming (SPIF) is an alternative to conventional reinforcement by means of stringers that are welded, riveted, or rigidly fastened to the surfaces of thin metallic panels. This type of reinforcement avoids the need of assembling operations and additional joining elements and eliminates the thermal-induced metallurgical changes and distortions that may compromise the final geometry and performance of the panels.

SPIF subjects the thin panels to in-plane stretching, and the deformation mechanics of groove stiffening can be analytically described by in-plane stretching of a shell assumed as a membrane, so that bending moments are neglected and forces are essentially transmitted through the sheet surfaces. The proposed analytical model is successfully utilized to determine the forming forces to produce the grooves and to estimate the maximum allowable groove depth before failure. Failure occurs by cracking along the longitudinal direction under opening mode I (by tension applied in the circumferential directions).

Comparisons against experimental measurements, finite element estimates, and alternative analytical models prove the effectiveness, simplicity, and very fast obtention of results by means of the new proposed analytical model.

ACKNOWLEDGMENTS

The authors would like to thank the support provided by Fundação para a Ciência e a Tecnologia of Portugal and IDMEC under LAETA-UIDB/50022/2020. Valentino A.M. Cristino would like to thank for the financial support of the University of Macau through the Start-up Research Grant SRG2019-00161-FST.

REFERENCES

[1] Klocke F (2013) Manufacturing Processes 4 – Forming. Springer, Aachen, Germany, 332-339.

[2] Köhler S, Rohnert C, Groche P (2018) Extension of geometric limits in drawing of stringer sheets, In (Eds. Mori KI, Abe Y, Maeno T) Proceedings of the 17th International Conference on Metal Forming - Metal Forming 2018, Toyohashi, Japan. Procedia Manufacturing 15: 693-700.

[3] Seguy S, Campa FJ, Lacalle LNL, Arnaud L, Dessein G, Aramendi G (2009) Toolpath dependent stability lobes for the milling of thin-walled parts. International Journal of Machining and Machinability of Materials 4: 377-392.

[4] Shamsuddin KA, Ab-Kadir AR, Osman MH (2013) A comparison of milling cutting path strategies for thin-walled aluminium alloys fabrication. International Journal of Engineering and Science 2: 1-8.

[5] Fusano L, Priarone PC, Avalle M, Filippi AM (2011) Sheet metal plate design: a structured approach to product optimization in the presence of technological constraints. International Journal of Advanced Manufacturing Technology 56: 31-45.

[6] Lacki P, Adamus J (2015) Numerical analysis of forming sheet panels with stiffening ribs. In (Eds. Oñate E, Owen DRJ, Peric D, Chiumenti M) Proceedings of the 13rd. International Conference on Computational Plasticity. Fundamentals and Applications – COMPLAS XIII, Barcelona, Spain, CIMNE 204-215.

[7] Eguia I, Mangas A, Iturbe R, Gutiérrez MA (2010) Electromagnetic forming of longitudinal strengthening ribs in roll formed automotive profiles. In (Eds. Babusci K, Daehn G, Marré M, Tekkaya AE, Weddeling C, Zhang Y). Proceedings of the 4th International Conference on High-Speed Forming—ICHSF 2010, Columbus, USA, 200-207.

[8] Slota J, Kubit A, Trzepiecinski T, Krasowski B, Varga J (2021) Ultimate load-carrying ability of rib-stiffened 2024-T3 and 7075-T6 aluminium alloy panels under axial compression. Materials 14: 1176.

[9] Cristino VAM, Pragana JPM, Bragança IMF, Silva CMA, Martins PAF (2021) Hybrid manufacturing of stiffening grooves in additive deposited thin parts. Journal of Manufacturing and Materials Processing 5: 140.

[10] ASTM E8/E8 M (2016) Standard Test Methods for Tension Testing of Metallic Materials; ASTM International: West Conshohocken, PA, USA.

[11] Silva MB, Nielsen PS, Bay N, Martins PAF (2011) Failure mechanisms in single-point incremental forming of metals. International Journal of Advanced Manufacturing Technology 56: 893–903.

[12] Martins PAF, Barata Marques MJM (1993) Plane strain rigid plastic finite element formulation for sheet metal forming processes. Journal of Engineering Manufacture 207: 167-171.

[13] Marciniak Z, Duncan JL (1992) The mechanics of sheet metal forming, 1st ed.; Edward Arnold, Auckland, New Zealand, 100-113.

[14] Chang ZD, Li M, Chen J (2019) Analytical modeling and experimental validation of the forming force in several typical incremental sheet forming processes. International Journal of Machine Tools and Manufacture 140: 62-76.

FIGURE CAPTIONS

Figure 1 (a) Stretching of thin panels and strengthening by means of (b) longitudinal 'T-shape' stringers and (c) longitudinal stiffening grooves.

Figure 2 True stress–strain curves of AISI 316L stainless steel sheets for the parallel (P), inclined (I) and transverse (T) directions with respect to the rolling directions.

Figure 3 Schematic representation and photograph of the experimental setup to fabricate the stiffening grooves by SPIF under laboratory conditions.

Figure 4 (a) Initial and (b) final computed meshes obtained from finite element analysis.

Figure 5 (a) Schematic representation of the stiffening groove with main notation; (b) the corresponding area of the local contact between the tool and the sheet placed immediately ahead.

Figure 6 Experimental, numerical, and analytical evolutions of the (a) cross-sectional geometry and (b) thickness of the stiffening groove for two different instants of time corresponding to a groove depth H of the semi-hemispherical tip tool equal to 5 mm and 11 mm

Figure 7 Principal strain space showing the experimental and finite element computed in-plane strains along the perimeter of the stiffening groove for an instant of time corresponding to a depth $H = 13$ mm immediately after cracking.

Figure 8 Evolution of the force per unit of length with the groove depth.

Figure 9 Experimental, numerical, and analytical evolutions of the tool force with the groove depth.

Table 1 Mechanical properties of the AISI 316L stainless-steel sheets.